Acoustic-phonon decoherence and electron transport in metallic nanostructures

2007 J. Phys.: Condens. Matter 19 216222

(http://iopscience.iop.org/0953-8984/19/21/216222)

IOP PUBLISHING JOURNAL OF PHYSICS: CONDENSED MATTER

J. Phys.: Condens. Matter **19** (2007) 216222 (12pp) doi:10.1088/0953-8984/19/21/216222

Acoustic-phonon decoherence and electron transport in metallic nanostructures

N Perrin

Laboratoire Pierre Aigrain, Ecole normale supérieure, 24 rue Lhomond, 75231 Paris 05, France

E-mail: Nicole.Perrin@lpa.ens.fr

Received 2 February 2007, in final form 14 February 2007
Published 2 May 2007
Online at stacks.iop.org/JPhysCM/19/216222

Abstract

In metallic quantum wires, electron transport at low temperatures (<10 K) is anticipated to be modified by acoustic-phonon confinement. This effect is investigated numerically through the dynamic conductance $\mathrm{d}J/\mathrm{d}E$. The role of the energy loss through the phonons from the wire to a substrate at $T_s = 0.4$ K is studied in cases of both strong (supported wire) and very weak (free-standing wire) acoustic coupling to the substrate characterized by the escape time τ_s. The phonons are shown to remain in the 1D regime until the electron energy is about 0.8 K, much smaller than the minimum mode-separation energy. The first subband essentially contributes to $\mathrm{d}J/\mathrm{d}E$ for a large phonon escape time τ_s, whereas for a small one it is impossible to distinguish the different modes. Finally, it is shown that the appearance of two peaks only in $\mathrm{d}J/\mathrm{d}E$, whatever the value of τ_s, results from the decoherence of phonons due to surface roughness. The case of single-walled carbon nanotubes is discussed.

1. Introduction

Transport phenomena have been extensively studied in nanoscale structures over the past decades, with a particular interest in the role of confined phonons. Confined optical phonons were first considered at rather high temperatures (200–300 K) and their scattering of electrons subsequently analysed either in semiconductor superlattices [1] or in quantum wires (QW) [2–5]. At low temperatures (∼15 K), Fasol *et al* [6] observed confined optical-phonon modes up to a high order in GaAs/AlAs quantum wells and examined the role of interface roughness on the dispersion. More recently, Yao *et al* [7] have shown that the current–voltage characteristics observed in metallic single-walled carbon nanotubes (SWNT) at different temperatures (4–200 K) can be explained by optical-phonon emission which is the dominant electron scattering mechanism at high fields. Though acoustic-phonon confinement was noted a long time ago in the early work of Grigoryan and Sedrakyan [8] in free-standing wires, acoustic phonons have received much less attention than optical phonons. Nevertheless, acoustic-phonon confinement has been studied theoretically by many

authors [9–14] in semiconductor QW or quantum wells with different geometries along with the electron-acoustic phonon scattering rates that dominate the electron scattering at low temperatures. In metallic nanostructures, the effect of acoustic-phonon confinement on the transport properties is an interesting problem from a fundamental point of view. It is also a somewhat puzzling problem [15], since the initial experimental investigations about the effects of phonon dimensionality on the electron–phonon relaxation time either in supported or in free-standing films [16, 17] at low temperatures ($\geqslant$0.5 K in the experiment of Di Tusa *et al* [16] and $\geqslant$1.4 K in those of Kwong *et al* [17]) have led to an open question rather than to a clear answer. More recently, besides the basic interest in phonons in intriguing carbon nanotubes, the role of acoustic phonons in the scattering of electrons in metallic single-walled carbon nanotubes at ambient temperature has been studied by several groups either theoretically [18] or experimentally [19]; the observed scattering rates at ambient temperature have shown that acoustic-phonon scattering is relevant at low biases [19]. The difficulties in the fabrication techniques [20] of nanowires are probably at the origin of the small number of experimental results in the field of mesoscopic phonon physics. Nevertheless, following Potts *et al* [21], Seyler and Wybourne [22] carried out experiments in supported metal Au wires at a substrate temperature $T_s = 1.2$ K and attributed the observed resonances in the electric resistance to the acoustic-phonon confinement and to the resulting reduced acoustic-phonon dimensionality. Their results disagree with the conclusions of Di Tusa *et al* [16] and Kwong *et al* [17]. Several authors [23, 24] claim that because of the width of the Bose–Einstein distribution compared to the average phonon energy, the contributions of the different acoustic-phonon subbands cannot be distinguished and the resolution of individual levels beyond the lowest-lying ones is not allowed.

In this paper we address the effect of phonon confinement on electron transport in metallic quantum wires at low temperatures ($<$10 K). When the wire is heated by an electric field, its conductivity is expected to be affected by the modifications of the phonon spectrum resulting from the spatial confinement of acoustic phonons. Confinement occurs when the phonon phase coherence length is larger than the lateral boundary separation d [25]. It is generally assumed that the temperature where the phonons get confined corresponds to a dominant phonon wavelength of the order of this lateral dimension; this is the dominant phonon-wavelength criterion. The resonances observed by Wybourne and his group in the resistance of electrically heated metal wires were assumed to be related to the acoustic modes in the wire. In their pioneering paper, Seyler and Wybourne [22] concluded that the periodicity of the resonances corresponds to an electron energy gain equal to the minimum subband spacing $v_s\pi/d$ with the emission of phonons in a higher acoustic subband of the wire (v_s is the sound velocity).

Another point to consider in the determination of the phonon spectrum and its relation to electron transport in a metallic wire is the rate of energy loss from the wire through the phonons. We characterize this loss by a phonon escape time τ_s. It has been shown experimentally [26] that the rate of energy loss from a film at low temperatures depends on the details of the phonon escape time. In the strong acoustic coupling limit between a supported wire and the substrate, the phonons remain nearly in equilibrium at a substrate temperature T_s and this implies a very short phonon escape time from the wire compared to the phonon relaxation time on the electrons. On the contrary, a weak acoustic coupling implies a large phonon escape time and heating of the phonon system by the electrons. The extreme case is a free-standing or self-supported wire. In the two latter cases, the departure of the stationary phonon distribution from a Bose–Einstein distribution at the substrate temperature is expected to be significant and to depend strongly on the phonon escape time. Therefore it seems that a weak acoustic coupling may provide the best conditions for phonon confinement; with strong acoustic coupling, the wire and the substrate together may behave as a single three-dimensional (3D) medium.

The above phonon escape time is a phenomenological representation of the local specular boundary scattering of phonons on the lateral surfaces of the wire. Moreover, real surfaces are known to be rough on the scale of hundreds of angstroms [27], i.e. the order of magnitude of the mean thermal phonon wavelength at 1 K. The surface irregularities must play an important role in phonon transport since the nature of the dispersion branches arises from the spatial quantization of the phonons determined by the free surfaces and the geometry of the wire. When surface roughness scattering is relevant [28], the phonons are expected to undergo partially diffuse scattering [29] as well as local specular scattering. In their experiments on suspended nanostructures, Tighe *et al* [30] showed that diffuse surface scattering is dominant from 1 to 10 K. According to the dominant phonon-wavelength criterion with $\lambda_{\mathrm{ph}} = hv_{\mathrm{s}}/(2kT)$ (k is the Boltzmann constant), size quantization and the related existence of acoustic-phonon subbands occur at low temperatures $T \ll 5$ K for lateral dimension ∼20 nm as a result of interference of the incident and specularly reflected waves. Increasing the phonon temperature from an initial value smaller than 1 K, the dominant phonon wavelength becomes of the order of magnitude of the surface asperities at $T \approx 1$ K. The resulting partially diffuse boundary scattering destroys the coherence with the incident wave and the subband structure may be partly removed. In this paper we will consider diffuse roughness scattering along with specular reflection; they are the major sources of acoustic-phonon scattering in a metallic wire besides electron scattering. They play quite different roles and may be more or less efficient according to the temperature. Spontaneous decay of phonons via three-phonon processes is assumed to be inefficient in nanowires [27].

Previously some parameters involved in the dynamic resistance of thin metallic wires with acoustic-phonon confinement have been analysed [31] in an attempt to determine the conditions required to observe features due to the phonon subbands at a temperature $T_{\mathrm{s}} = 400$ mK. As far as the phonon dimensionality is concerned, it has been shown that the phonons are of intermediate dimension between 2 and 3. It has also been shown in a first comparison with experiments [32] at $T_{\mathrm{s}} = 50$ mK that by numerical calculations it seems possible to get structures similar to those experimentally observed for the electron resistance; however, no straightforward relationship between the electron temperature of the single dynamic conductance maximum obtained and the temperature corresponding to the mode separation energy at the zone centre has been pointed out.

In this paper, we analyse the contribution of the acoustic-phonon subbands to the electron transport in a AuPd wire heated by an electric field; we consider different acoustic couplings to the substrate with different phonon escape times. We also analyse the role of surface roughness and the way the loss of phonon coherence affects the electron transport.

2. Model

2.1. Phonon modes

We consider metallic wires of rectangular cross section deposited on a substrate at a temperature $T_{\mathrm{s}} = 400$ mK. The width $d = 20$ nm and thickness $b = d/3$ are small enough so that acoustic phonons get confined with a dominant wavelength $\lambda_{\mathrm{ph}} = hv_{\mathrm{s}}/(2kT_{\mathrm{s}}) \approx 250\ \mathrm{nm} \gg d$. It is well known that an analytical solution of the field equations with appropriate boundary conditions has not been found for a rectangular quantum wire [33] and that Morse's ansatz [34] with approximate hybrid modes calculated assuming separable boundary conditions has often been used. However, the normal modes of acoustic phonons have been precisely calculated using a so-called *xyz* algorithm [35] that points out the existence of edge modes at the wire corners. We use here the hybrid modes corresponding to the width and thickness of the wire with an aspect

ratio $d/b = 3$ to simplify the calculation, hence missing the edge modes. Therefore, we write the following dispersion relationship [33]:

$$\omega^2 = v_s^2 \left[\beta^2 + \left(\frac{n\pi}{d}\right)^2 + \left(\frac{m\pi}{b}\right)^2 \right] = v_s^2 \left[\beta^2 + q_\perp^2\right] = v_s^2 \beta^2 + \omega_{nm}^2 \tag{1}$$

where β is the longitudinal phonon wavevector along the length L of the wire. The integers n and m are the subband indices. The lowest vibration mode $n = m = 0$ has a linear dispersion with a transverse wavevector $q_\perp = 0$ without a frequency gap at $q = 0$. From (1), we deduce the density of states $g_{nm}(\omega)$:

$$g_{nm}(\omega) = (2\pi d b v_s)^{-1} \omega \, (\omega^2 - n^2\omega_{od}^2 - m^2\omega_{ob}^2)^{-1/2} = (2\pi d b v_s)^{-1} \omega \, (\omega^2 - \omega_{nm}^2)^{-1/2} \tag{2}$$

$\omega_{od} = \pi v_s/d$ and $\omega_{ob} = \pi v_s/b$ are the cut-off frequencies characteristic of the width and thickness modes, respectively, of the wire. At the frequency $\omega_{nm} = (n^2\omega_{od}^2 + m^2\omega_{ob}^2)^{1/2}$ a singularity appears in the density of states: it becomes infinite and the group velocity $v_g = \mathrm{d}\omega/\mathrm{d}\beta = v_s\omega^{-1}(\omega^2 - \omega_{nm}^2)^{1/2}$ is then equal to zero.

2.2. Electron temperature

We assume an effective electron temperature T_e resulting from electron–electron thermalizing collisions that do not contribute to the energy losses from the electron gas. From the Sommerfeld expansion [36] of the internal-energy density of the Fermi electron gas in the presence of an electric field E, T_e satisfies the equation:

$$(kT_e)^2 = (kT_s)^2 + 6\pi^{-2}(eEl_i)^2 \qquad \text{with } l_i = (D\tau_i)^{1/2} \quad \text{whenever } l_i < L \tag{3}$$

$D = v_f^2\tau_e/3$ is the inelastic diffusion constant, v_f is the Fermi velocity, τ_e is the electron elastic relaxation time and τ_i is the energy-loss lifetime [37]. The term eEl_i represents the energy gained by an electron during its diffusion over l_i through the disordered metal. The scattering of the electrons by the acoustic phonons is assumed to be the dominant source of inelastic scattering. In these conditions, the energy relaxation time at low temperatures can be written as a power law of T_e [38, 39] resulting in an inelastic diffusion length l_i that depends on the phonon dimensionality p:

$$l_i = (D\alpha_i)^{1/2} T_e^{-p/2} = \chi T_e^{-p/2} \qquad \text{with } \tau_i = \alpha_i T_e^{-p} \tag{4}$$

where χ is a constant.

2.3. Electron dynamic conductance and phonon power balance

The power absorbed by the electrons from the electric field scales with the resistivity ρ that is controlled by the elastic temperature-independent impurity scattering. In the steady state, the power per volume F absorbed by the electrons is entirely transmitted to the phonon system; following the approach initially introduced by Perrin and Budd [40], we can therefore write the balance equation involving the phonon relaxation times and the different subbands:

$$\frac{E^2}{\rho} = JE = \sum_{nm} \left[\int \mathrm{d}\omega \hbar\omega g_{nm}(\omega) \frac{N(\omega, T_e) - N(\omega, T_s)}{\tau_s(\omega) + \tau_{ep}(\omega)} \right] = \sum_{nm} (JE)_{nm} = \sum_n F_n = F. \tag{5}$$

$N(\omega, T)$ is the Bose distribution at T. The energy relaxation time on the electrons τ_{ep} given by Pippard [41] and valid whatever ql_e is independent of the electron temperature T_e. The phonon escape time is assumed to be of the form $\tau_s(\omega) = \tau_{so}(x) f(n, \omega)$ with $\tau_{so}(x) = \eta_o x/v_s$; for the fundamental mode, $x = L$ and for the modes (nm), $x = d$. The acoustic parameter η_o is a

constant and the dependence of the escape time on the phonon subband is introduced through the function $f(n, \omega) = \omega/(n\omega_{od})$ [31]: we assume a mean phonon escape time independent of m and b.

We will investigate the dynamic conductance dJ/dE deduced from (5):

$$\frac{dJ}{dE} = E^{-1}\,(dT_e/dE)(dF/dT_e) - \left(F/E^2\right) = \sum_n (dJ/dE)_n = \sum_n \left[\sum_m (dJ/dE)_{nm}\right]. \quad (6)$$

The roughness of the surface is introduced through a T_e-dependent function $0 < p_n < 1$ that filters the power F_n stored in the different confined modes: $p_n = 1$ for mirror like scattering without any modification of F_n; $p_n = 0$ in the diffuse scattering limit. According to Ziman [29], we assume:

$$p_n = \exp(-w_n) \qquad \text{with } w_n = 4\pi^3 (h_a/d)^2 \left[5kT_e/(n\hbar\omega_{od})\right]^2 \quad (7)$$

where w_n depends on the ratio h_a/d of the height h_a of the surface asperities to the width d of the wire. The expression $(kT_e/d\hbar\omega_{od})$ in (7) comes from the wavelength dependence of w_n introduced by Ziman assuming $\lambda = 2\pi\hbar v_s/kT_e = 2\hbar\omega_{od}/kT_e d$. With the wire constants considered here, we get $\hbar\omega_{od} \approx 5$ K and $5kT_e/\hbar\omega_{od} \approx 1$ at $T_e = 1$ K. The roughness parameters are not known but they can be estimated from localization studies in free-standing nanostructures [42] or from thermal conductance [28, 30].

3. Results and discussion

3.1. Phonon coherence and phonon escape time

We have performed the numerical calculations for a rectangular wire of length $L = 5$ mm assuming a mean sound velocity $v_s = 4.2 \times 10^3$ m s^{-1} and an elastic electron mean free path $l_e = 20$ nm. Therefore, for a Fermi velocity $v_f = 1.4 \times 10^6$ m s^{-1}, the value of the inelastic diffusion constant is $D \approx 10^3$ m^2 s^{-1}; the resulting inelastic mean free path l_i is about a few micrometres ($\approx 2\ \mu$m) with a phonon dimensionality $p = 1.3$ according to previous results and $\chi = 2 \times 10^{-6}$ deduced from experimental results [31].

In figures 1 and 2, we show the calculated individual modes $(dJ/dE)_{nm}$ as a function of T_e obtained with the acoustic parameter $\eta_o = 2000$ and 20 respectively and with $m = 0$. For both values of η_o, the successive results $\sum_n (dJ/dE)_n$ with n increasing from $n = 0$ to n_{max} chosen in our calculations, are shown in the inset: the solid line gives the characteristic behaviour of the dynamic conductance dJ/dE resulting from the contribution of the different modes considered (curve 'sum' in the main figure). When the three first values of m are introduced in the calculations instead of the case $m = 0$ considered here, the variations obtained in dJ/dE are not significant [31] at least at low temperature. The common feature of the curves $(dJ/dE)_{nm}$ corresponding to the confined modes ($n \neq 0$) is the occurrence of a maximum for a value $T_{en}(\eta_o)$ of the electron temperature, which is an increasing function of n as expected; but for a given n, $T_{en}(\eta_o = 2000) < T_{en}(\eta_o = 20)$ and the height of the peak is as small as η_o is large. For $\eta_o = 2000$, the resulting curve dJ/dE exhibits but one maximum at $T_e \approx 0.9$ K, i.e. a value slightly larger than the position at 0.8 K of the peak of the first mode $n = 1$. Its width reaches rapidly a limit smaller than 2 K when the number of modes is increased, as is seen in the inset. In contrast, for $\eta_o = 20$, dJ/dE spreads over an electron temperature range as large as the number of modes included is large. It also exhibits a maximum at $T_e \approx 0.9$ K, and either a bump or a second maximum at a temperature $T_e > 0.9$ K. The position of the latter is shifted towards higher values of T_e as n increases. For both values of η_o the peak at $T_e \approx 0.9$ K essentially results from the contribution of the first calculated confined mode $n = 1$.

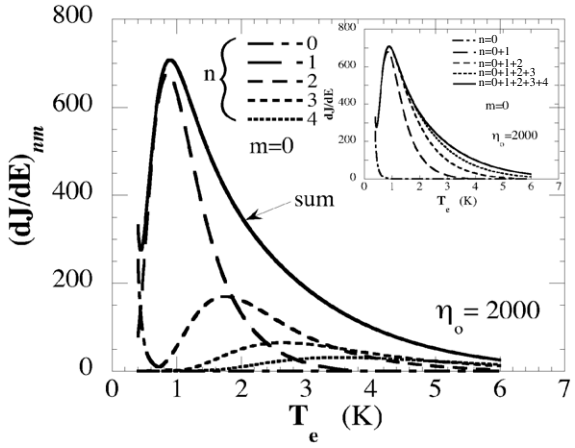

Figure 1. Contribution $(\mathrm{d}J/\mathrm{d}E)_{nm}$ of the first successive subbands $n = 0$–4 ($m = 0$) to the dynamic conductance (SI units) and their sum (solid line) for an acoustic parameter $\eta_o = 2000$. The successive results $\sum_n (\mathrm{d}J/\mathrm{d}E)_{nm}$ from $n = 0$ to 4 are shown in the inset.

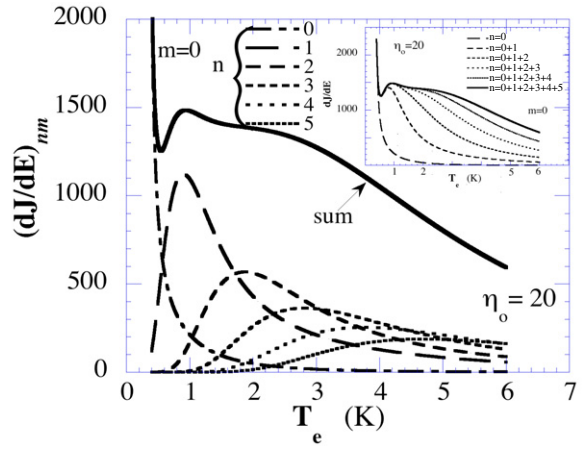

Figure 2. Contribution $(\mathrm{d}J/\mathrm{d}E)_{nm}$ of the first successive subbands $n = 0$–5($m = 0$) to the dynamic conductance (SI units) and their sum (solid line) for an acoustic parameter $\eta_o = 20$. The successive results $\sum_n (\mathrm{d}J/\mathrm{d}E)_{nm}$ from $n = 0$ to 5 are shown in the inset.

To explain these results, it is interesting to consider the non-equilibrium phonon distribution rate $[N(T_e) - N(T_s)]/[\tau_s(\omega) + \tau_{ep}(\omega)]$ in (5), that depends on T_e through $N(T_e)$ only, and the involved relaxation times $\tau_s(\omega)$ and $\tau_{ep}(\omega)$. These times are shown in figure 3 for both values of η_o. For $\eta_o = 2000$, the escape time $\tau_s(\omega)$ is shown for the subbands $n = 1$ and 2 along with $\tau_{so}(x = d)$. They satisfy the relations $\tau_{so}(d) = \tau_{ep}(\omega \approx 100 \times 10^{10}\ \mathrm{s}^{-1})$ and $\tau_s(\omega) \geqslant \tau_{ep}(\omega)$ for $\omega > 80 \times 10^{10}\ \mathrm{s}^{-1}$ for the subband $n = 1$. The behaviour of this subband is then essentially determined by $\omega N(T_e)/\tau_s(\omega)$. On the contrary for $\eta_o = 20$, the behaviour of the subbands is determined by $\omega N(T_e)/\tau_{ep}(\omega)$ over a large range of frequencies $\omega_{od} \leqslant \omega \leqslant 6\omega_{od}$ for $n = 1$ and over a still larger range for $n = 2$. In the steady state, the rate of change with the electron temperature $\mathrm{d}F/\mathrm{d}T_e$ of the power F per volume (5) transferred from the electrons to the phonons must be equal to the rate of change of the power absorbed by the electrons from the field $\gamma T_e/\tau_{el}(T_e)$. By equating these two rates:

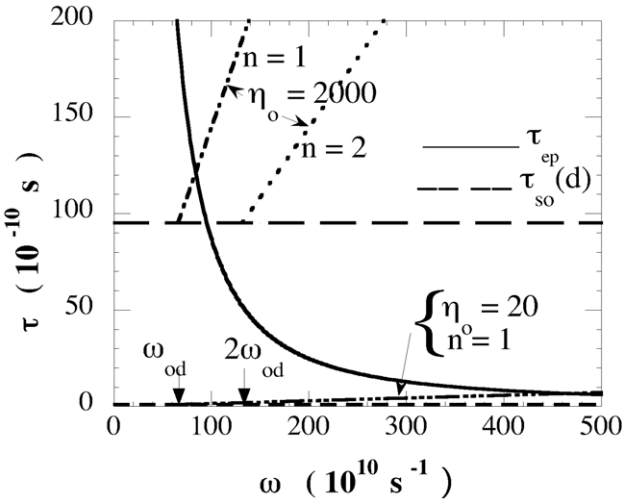

Figure 3. Phonon relaxation time on the electrons τ_{ep} (solid line) and phonon escape time τ_s for the subbands $n = 1$ (dashed–dotted line) and $n = 2$ (dotted line) versus the phonon frequency ω. $\tau_{so}(d) = \eta_o d/v_s$ (dashed line) is independent of the subband.

$$dF/dT_e = \sum_{nm} \left\{ \int d\omega \hbar\omega g_{nm}(\omega) \left[\tau_s(\omega) + \tau_{ep}(\omega)\right]^{-1} \left[dN(T_e)/dT_e\right] \right\} = \gamma T_e/\tau_{el}(T_e) \tag{8}$$

we obtain the electron energy relaxation rate $\tau_{el}^{-1}(T_e)$; it depends on the phonon relaxation times, on T_e and on the electron specific heat γ. Using the probing function $P(\omega)$ first introduced by Kanskar [43],

$$P(\omega) = \frac{\omega^2}{\tau_s(\omega) + \tau_{ep}(\omega)} \mathrm{sh}^{-2}\left[\hbar\omega/(2kT_e)\right] \tag{9}$$

the electron energy-relaxation rate $\tau_{el}^{-1}(T_e)$ can be written as:

$$\tau_{el}^{-1}(T_e) = \frac{\hbar^2}{4k\gamma T_e^3} \sum_{\text{modes}} \left[\int d\omega\, g_{nm}(\omega) P(\omega) \right]. \tag{10}$$

Therefore, the phonon function $P(\omega)$ characterizes the rate of energy transfer from the electrons to the phonons at a temperature T_e. The function $P_o(\omega)$ obtained with $\tau_s(\omega) = \tau_{so}(d) = \eta_o d/v_s$ is shown in figure 4 for different temperatures $T_e = 0.6, 0.7, 0.8$ and 1 K and for both values of η_o: $\eta_o = 2000$ and $\eta_o = 20$. As T_e is increased, the curves spread over a larger range of frequencies whatever the value of η_o, and phonon frequencies $\omega > \omega_{od}$ are involved in $P_o(\omega)$ as soon as T_e reaches 0.7 K. For $\eta_o = 2000$, the contribution of these frequencies to the integral in (10) remains small until $T_e \approx 0.8$ K where the half-height value of the curve $P(\omega)$ occurs at $\omega = \omega_{od}$. After that frequencies larger than ω_{od} become important in (10) and therefore in the energy transfer from the electrons to the phonons. The subband $n = 1$ begins to be excited, whereas for $T_e \leqslant 0.8$ K the electron energy relaxes towards the 1D phonon system with just the lowest order channel $n = 0$ involved. It is also seen in figure 4 that the curves $P_o(\omega)$ with both values of η_o are close together for low values of T_e (0.6–0.7 K) but they split apart as T_e increases. According to the quite different values of the ratio $\tau_{ep}/\tau_{so}(d)$ in (9), the curve with $\eta_o = 20$ is always above the curve with $\eta_o = 2000$. It is also larger as soon as $T_e \geqslant 0.7$ K. The phonon system with a small escape time τ_s quickly loses its 1D nature as T_e increases from its initial value $T_e = T_s$. These results are

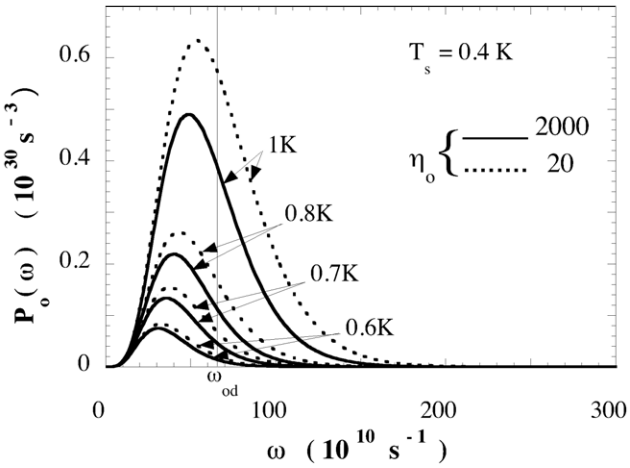

Figure 4. The function $P_o(\omega)$ with $\tau_s(\omega) = \tau_{so}(d)$, characteristic of the rate of energy transfer from the electrons to the phonons, shows that the subband $n = 1$ begins to be excited at $T_e \approx 0.8$ K for $\eta_o = 2000$ whereas for $\eta_o = 20$ it is excited for lower temperatures.

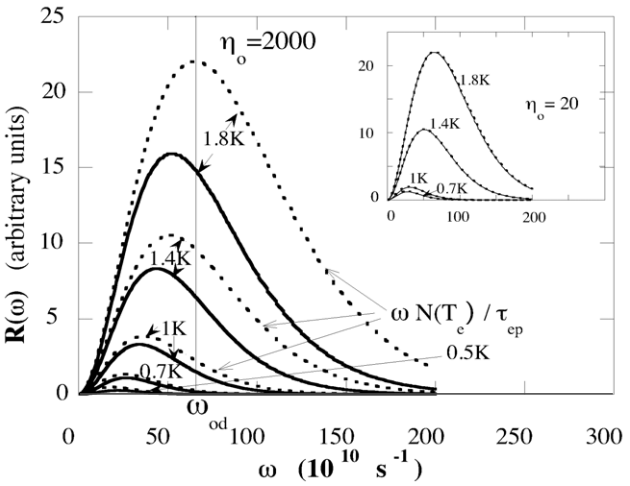

Figure 5. Comparison of the function $R(\omega) = \omega[N(T_e) - N(T_s)]/[\tau_s(\omega) + \tau_{ep}(\omega)]$ with $\eta_o = 2000$ to $R_B(\omega) = \omega N(T_e)/\tau_{ep}(\omega)$. The same comparison is shown in the inset with $\eta_o = 20$; the importance of the phonon escape time is clearly seen.

confirmed by the analysis of the curves in figure 5 where we show the relevant phonon function $R(\omega) = \omega[N(T_e) - N(T_s)]/[\tau_s(\omega) + \tau_{ep}(\omega)]$ in the expression (5) of the power per volume F and the function $R_B(\omega) = \omega N(T_e)/\tau_{ep}(\omega)$ for comparison. For $\eta_o = 2000$, i.e. a large acoustic mismatch between the film and the surrounding medium and therefore a nearly free-standing nanostructure, we observe an important discrepancy between the curves for $T_e \geqslant 1$ K; with $\tau_{ep}(\omega) < \tau_s(\omega)$ as seen in figure 3, the phonons of the subband $n > 2(\omega \geqslant 2\omega_{od})$ are roughly in thermal equilibrium with the electrons and do not receive any energy. The subband $n = 2$ begins to be populated by the relaxation energy of the electrons at $T_e \approx 1.4$ K. On the contrary,

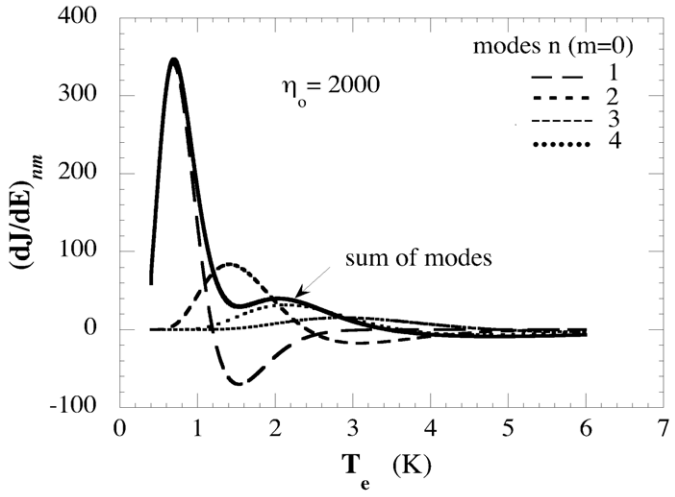

Figure 6. Separate contributions of the subbands $n = 1$–4 (dashed and dotted lines) and the resulting $\mathrm{d}J/\mathrm{d}E$ (solid line, SI units) with a large phonon escape time in the presence of surface roughness that results in phonon decoherence.

for $\eta_o = 20$ (inset of figure 5), $R(\omega)$ (full line) and $R_B(\omega)$ (dotted line) are the same but at temperatures $T_e \leqslant 0.7$ K where they exhibit a small difference; with $\tau_s(\omega) < \tau_{ep}(\omega)$ (figure 3), the phonons of the subbands $n \geqslant 2$ are in thermal equilibrium at $T_s = 0.4$ K for $T_e > 0.7$ K: the 3D phonon system is given a large amount of energy by the emitting electrons.

An interesting result is that, contrary to what was thought in the early studies [22], the temperature ≈0.8 K required for the emission of phonons by the electrons in the first subband $n = 1$ is much lower than the temperature corresponding to the mode separation energy $\hbar\omega_{od} \approx 5$ K at $\beta = 0$ in the wire considered here.

From the above discussion, we can explain both the maximum observed in $\mathrm{d}J/\mathrm{d}E$ (figure 1, namely $\eta_o = 2000$, and figure 2, namely $\eta_o = 20$) essentially due to the first subband $n = 1$ and the very small contribution of the higher subbands for $\eta_o = 2000$. We have also pointed out the transition from the 1D regime to the 3D regime for $\eta_o = 20$ and the important contribution of the higher subbands that is clearly seen in figure 2. However, the contributions of the different acoustic-phonon subbands $n > 1$ to $\mathrm{d}J/\mathrm{d}E$ cannot be distinguished for $\eta_o = 20$ and the resulting bump in figure 2 must be attributed to whole modes $n > 1$.

3.2. Surface roughness and phonon decoherence

Figures 6 and 7 show the calculated individual modes $(\mathrm{d}J/\mathrm{d}E)_{nm}$ of the dynamic conductance with $m = 0$ and the successive values of n ($n = 1$–4) for both values of η_o, 2000 and 20 when the power F_n stored in the confined modes is limited as a result of surface roughness and diffuse scattering. The solid line is the sum over n of the modes considered: it shows the characteristic behaviour of the dynamic conductance $\mathrm{d}J/\mathrm{d}E$ when diffuse scattering is present. We assume the height of the asperities $h_a = 0.4$, $d = 80$ Å. In figure 6 ($\eta_o = 2000$), it is seen that the peaks of the modes $n = 1$ and 2 are quite distinct, contrary to figure 1 and in contrast to the peak of the mode $n = 3$ which is quite close to the curve $(\mathrm{d}J/\mathrm{d}E)_{n=2,m=0}$ but not overlapped by the curve $n = 2$ as in figure 1. The curves obtained with (7) exhibit oscillations and are narrower than the corresponding curves in figure 1. Roughness in this case leads to a splitting of the first two modes but not of the other modes that contribute very little to $\mathrm{d}J/\mathrm{d}E$. In figure 7, with a

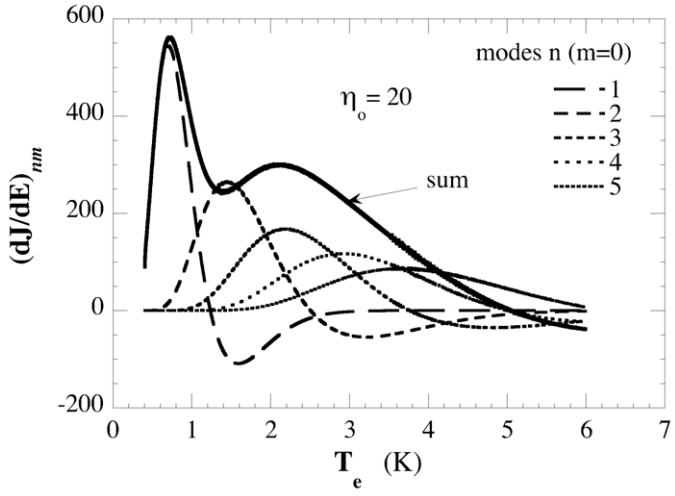

Figure 7. Separate contributions of the subbands $n = 1$–5 (dashed and dotted lines) and the resulting $\mathrm{d}J/\mathrm{d}E$ (solid line, SI units) with a small phonon escape time in the presence of surface roughness that results in phonon decoherence.

good coupling of the phonons to the surrounding medium ($\eta_o = 20$) and a small escape time, the three first peaks are rather well separate. However, as in the previous case of a large phonon escape time, we see but two peaks in $\mathrm{d}J/\mathrm{d}E$. The phonon decoherence is more efficient for a large phonon escape time; it enhances the relative importance of the first confined mode.

The phonon decoherence must still be enhanced in true free-standing nanostructures that correspond to an upward limit of a very large phonon escape time. For a small phonon escape time, the phonon system is already in interaction with the surrounding medium and surface roughness enlarges the decoherence of the phonon system.

4. Conclusion

We have investigated the electron dynamic conductance $\mathrm{d}J/\mathrm{d}E$ in metallic nanowires at low temperatures ($T_e = 0.4$–7 K) where the acoustic phonons exhibit reduced-dimensional behaviour. We have used the phonon dispersion relationship for a rectangular wire obtained within the hybrid modes approximation. The electron dynamic conductance has been expressed as a function of the phonon parameters and we have calculated the contribution $(\mathrm{d}J/\mathrm{d}E)_{nm}$ of each subband $(n, m = 0)$, the thickness modes being negligible at low temperatures [31]. According to the dominant phonon-wavelength criterion, the phonons are anticipated to remain in the 1D regime until the electron energy reaches $\hbar\omega_{\mathrm{od}}$, i.e. a temperature of about 5 K for the wire considered here. In this paper, we have shown that the mode separation energy at the centre of the zone is not the energy required to get phonons emitted by the electrons in the first subband $n = 1$; this subband begins to be excited at a temperature $T_e \approx 0.8$ K for a large phonon escape time. Our results agree with the experiments of Schwab *et al* [24] in suspended insulating nanostructures of lateral dimensions <100 nm where the thermal conductance measured with decreasing temperature is seen to reach the one-dimensional limit at $T_e \approx 0.8$ K. When the phonon escape time is small, a phonon transition from the 1D to the 3D regime is clearly seen. In the latter case all the phonon modes are excited by the electrons and contribute to $\mathrm{d}J/\mathrm{d}E$, but it is impossible to distinguish their individual contributions. The modes $(\mathrm{d}J/\mathrm{d}E)_{nm}$ cannot

be separated. For a large phonon escape time, we have shown that dJ/dE is essentially the contribution of the first subband.

When surface roughness is taken into account, we have shown that the behaviour of dJ/dE depends on the phonon escape time. For a large phonon escape time, we can see two separate peaks in figure 6, the first mode $n = 1$ being largely enhanced relative to the mode $n = 2$. For a small escape time we also see two peaks, the first one corresponding to the mode $n = 1$ whereas the second one results from the sum over the modes $n > 1$. Therefore the phonon decoherence occurring in the metallic wire and due to surface roughness leads in the end to the appearance of two peaks only in dJ/dE, whatever the phonon escape time.

The above calculations apply to single-wall carbon nanotubes. Indeed, by measuring the temperature-dependent specific heat of purified SWNT, Hone *et al* [44] have shown direct evidence of 1D quantized phonon subbands. These subbands result from the splitting of each of the four acoustic bands (one longitudinal, two transverse and one torsional) [45] due to the periodic boundary conditions on the circumferential wavevector. The small size and the high phonon velocity result in a much larger energy splitting between phonon subbands than in the metallic nanowires considered above; it may reach 30 K for the first subband of a (10, 10) tube of diameter 1.25 nm [44]. At low temperatures only the acoustic subbands are populated. The electron–phonon coupling has been shown to be strong for the longitudinal mode in suspended SWNT [46]. The contributions to the conductance of the different subbands with small longitudinal wavevector β are expected to be easily separated when the temperature is increased, as has been shown in current–voltage characteristics in recent transport experiments by Sapmaz *et al* [46]. The main causes of roughness in SWCN are defects and small variations of the tube diameter. Recently, chemical processes of purification and dispersion have been addressed [47]; they result in very pure SWCN. With these techniques the decoherence of phonons in SWCN may be expected to be monitored in future investigations.

Acknowledgments

The author would like to thank Professor M N Wybourne for having attracted her attention on the experimental results and problems connected with electron transport in metallic nanostructures with acoustic-phonon confinement. She also thanks the University Pierre and Marie Curie Paris for making this work possible as an Emeritus Professor.

References

[1] Mori N and Ando T 1989 *Phys. Rev.* B **40** 6175–88
[2] Constantinou N C and Ridley B K 1990 *Phys. Rev.* B **41** 10622–6
[3] Kim K W, Stroscio M A, Bhatt A, Mickevicius R and Mitin V V 1991 *J. Appl. Phys.* **70** 319–27
[4] Mickevicius R, Mitin V V, Kim K W, Stroscio M A and Iafrate G J 1992 *J. Phys.: Condens. Matter* **4** 4959–70
[5] Enderlein R 1993 *Phys. Rev.* B **47** 2162–75
[6] Fasol G, Tanaka M, Sakaki H and Horikoshi Y 1988 *Phys. Rev.* B **38** 6056–65
[7] Yao Z, Kane C L and Dekker C 2000 *Phys. Rev. Lett.* **84** 2941–4
[8] Grigoryan V G and Sedrakyan D G 1983 *Sov. Phys. Acoust.* **29** 281–3
[9] Nishiguchi N 1994 *Japan. J. Appl. Phys.* **33** 2852–8
Nishiguchi N 1994 *Phys. Rev.* B **50** 10970–80
[10] Yu S, Kim K W, Stroscio M A, Iafrate G J and Ballato A 1994 *Phys. Rev.* B **50** 1733–8
[11] Yu S, Kim K W, Stroscio M A and Iafrate G J 1995 *Phys. Rev.* B **51** 4695–8
[12] Nishiguchi N 1996 *Physica* B **219/220** 40–2
[13] Mitin V V, Vasko F T, Bannov N A and Stroscio M A 1996 *Physica* B **219/220** 34–6
[14] Mittal A 1996 *Quantum Transport in Semiconductor Submicron Structures* (*NATO Advanced Study Institute, Series E: Applied Science*) ed B Kramer (Dordrecht: Kluwer) pp 303–13

[15] Bergman G, Wei W, Zou Y and Mueller R M 1990 *Phys. Rev.* B **41** 7386–96
[16] DiTusa J F, Lin K, Park M, Isaacson M S and Parpia J M 1992 *Phys. Rev. Lett.* **68** 1156–9
[17] Kwong Y K, Lin K, Isaacson M S and Parpia J M 1992 *J. Low Temp. Phys.* **88** 261–72
[18] Suzuura H and Ando T 2002 *Phys. Rev.* B **65** 235412–26
[19] Park J, Rosenblatt S, Yaish Y, Sazonova V, Üstünel H, Braig S, Arias T A, Brouwer P W and McEuen P L 2004 *Nano Lett.* **4** 517–20
[20] Lee K L, Ahmed H, Kelly M J and Wybourne M N 1984 *Electron. Lett.* **20** 289
[21] Potts A, Kelly M J, Hasko D G, Cleaver J R A, Ahmed H, Ritchie D A, Frost J E F and Jones G A C 1992 *Semicond. Sci. Technol.* B **7** 231
[22] Seyler J and Wybourne M N 1992 *Phys. Rev. Lett.* **69** 1427–30
[23] Blencowe M 2004 *Phys. Rep.* **395** 159–222
[24] Schwab K, Arlett J L, Worlock J M and Roukes W M 2001 *Physica* E **9** 60–8
[25] Wybourne M N 1996 *Physica* B **219/220** 13–5
[26] Nabity J C and Wybourne M N 1990 *J. Phys.: Condens. Matter* **2** 3125–9
[27] Perrin N 1993 *Phys. Rev.* B **48** 12151–4
[28] Santamore D H and Cross M C 2002 *Phys. Rev.* B **66** 144302–20
[29] Ziman J M 1960 *Electrons and Phonons* (Oxford: Clarendon) p 456
[30] Tighe T S, Worlock J M and Roukes M L 1997 *Appl. Phys. Lett.* **70** 2687–9
[31] Perrin N 1999 *Physica* B **263/264** 498–500
[32] Perrin N and Wybourne M N 1996 *Physica* B **219/220** 37–9
[33] Auld B A 1973 *Acoustic Fields and Waves in Solids* vol 2 (New York: Wiley) p 114
[34] Morse R W 1948 *J. Acoust. Soc. Am.* **20** 833–8
[35] Nishiguchi N, Ando Y and Wybourne M N 1997 *J. Phys.: Condens. Matter* **9** 5751–64
[36] Ashcroft N W and Mermin N D 1976 *Solid State Physics* (Philadelphia, PA: Holt, Rinehart and Winston) pp 45–6
[37] Bergmann G 1990 *Solid State Commun.* **75** 605–7
[38] Anderson P W, Abrahams E and Ramakrishnan T V 1979 *Phys. Rev. Lett.* **43** 718–20
[39] Arai M R 1983 *Appl. Phys. Lett.* **42** 906–8
[40] Perrin N and Budd H 1972 *Phys. Rev. Lett.* **28** 1701–3
Perrin N and Budd H 1972 *J. Phys. C: Solid State Phys.* **33** C4 33–9
[41] Pippard A B 1955 *Phil. Magn.* **46** 104
[42] Blencowe M P 1995 *J. Phys.: Condens. Matter* **7** 5177–93
[43] Kanskar M 1994 *PhD Thesis* University of Oregon, unpublished
[44] Hone J, Batlogg B, Benes Z, Johnson A T and Fisher J E 2000 *Science* **289** 1730–3
[45] Saito R, Takeya T, Kimura T, Dresselhauss S and Dresselhaus M S 1998 *Phys. Rev.* B **57** 4145–53
[46] Sapmaz S, Jarillo-Herrero P, Blanter Ya M, Dekker C and van der Zant H S J 2006 *Phys. Rev. Lett.* **96** 26801–4
[47] Wang Y, Gao L, Sun J, Liu Y, Zheng S, Kajiura H, Li Y and Noda K 2006 *Chem. Phys. Lett.* **432** 205–8